

Article

# Systematic Analysis of Materials for Coated Adsorbers for Application in Adsorption Heat Pumps or Refrigeration Systems

Oscar Banos <sup>1,\*</sup> , Sven Ohmann <sup>1</sup>, Felix Alscher <sup>1</sup>, Cornelia Breitkopf <sup>1,\*</sup> , Vicente Pacheco <sup>2</sup>, Maja Glorius <sup>1</sup>  and Matthias Veit <sup>1</sup>

<sup>1</sup> Chair of Technical Thermodynamics, Institute of Power Engineering, Faculty of Mechanical Science and Engineering, Technische Universität Dresden, 01069 Dresden, Germany; Sven.Ohmann@tu-dresden.de (S.O.); Felix.Alscher@tu-dresden.de (F.A.); Maja.Glorius@tu-dresden.de (M.G.); Matthias.Veit@tu-dresden.de (M.V.)

<sup>2</sup> Fraunhofer Institut IFAM, 28359 Dresden, Germany; vicente.pacheco@ifam-dd.fraunhofer.de

\* Correspondence: Oscar.Banos\_Garcia@tu-dresden.de (O.B.); Cornelia.Breitkopf@tu-dresden.de (C.B.)

Received: 19 August 2020; Accepted: 17 September 2020; Published: 22 September 2020



**Abstract:** Water vapor sorption in salt hydrates is a promising method to realize seasonal solar heat storage. Several of these materials have already shown promising performance for this application. However, a significant bottle neck for applications is the low thermal conductivity. In this study, several fabrication methods of the fixation of salts and their hydrates on metals to overcome the problem are presented. The products are analyzed concerning the hydration states, the corrosion behavior, the chemical compatibility, and the mechanical stability.

**Keywords:** hydrates; adsorption; energy storage; refrigeration; heat pumps; composites

## 1. Introduction

Recent research on heat pumps, refrigeration systems, and heat storage materials has mainly focused on developing environmentally friendly new systems that perform with high efficiency and are able to employ various kinds of primary energy [1]. Among these, adsorption-based devices are of special interest because of the great variety of adsorbents, which allow the optimal selection of application according to the desired temperature levels, including low temperature heat sources such as solar thermal energy or waste heat.

Adsorption refrigeration systems are based upon a batch working principle where adsorption and desorption are combined alternatively [2,3]. The working fluid (usually water, ammonia, or methanol) is evaporated at the lowest temperature using the heat of evaporation  $Q_{\text{eva}}$ . Because adsorption (of vapor) is an exothermic process, the enthalpy of adsorption is released at a medium temperature. The principle of the thermodynamic cycle is shown in Figure 1.2 of [2]. During the regeneration process, the vapor is desorbed by applying the regeneration heat  $Q_{\text{h}}$  from the external heat source (the driving heat). The working fluid is then condensed, releasing the heat  $Q_{\text{cond}}$ . In refrigeration systems, the useful effect is produced in the evaporator by taking  $Q_{\text{eva}}$  from the user device, while  $Q_{\text{cond}}$  and  $Q_{\text{ad}}$  are dissipated to the environment. In heating pumps, the heat values  $Q_{\text{cond}}$  and  $Q_{\text{ad}}$  are the useful outputs and  $Q_{\text{eva}}$  is taken from the environment. For adsorption heat storage applications, the energy  $Q_{\text{h}}$  is stored during the endothermic desorption and released during the exothermic adsorption  $Q_{\text{ad}}$ .

Among the commonly used working pairs, water is always the preferred choice of sorbate because of its safety and low cost, while ammonia and ethanol are the most feasible candidates for ice making and very low temperatures [4]. However, the variety of commonly used adsorbent classes for adsorptive energy storage systems is limited. Activated carbon, zeolite, and silica gel are

mostly used [5,6]. New potential adsorbent materials include silico-alumino-phosphates (SAPO) and alumino-phosphates (ALPO) [7–9], in addition to MOFs (metal organic frameworks), such as 101-MIL, which have high net water uptakes [10,11]. Among the new adsorbates, extensive research on salt hydrates has been carried out for possible use in thermal storage processes. The main reasons to use salt hydrates are a high theoretical energy density of the materials and desorption temperatures achievable with waste heat sources and solar thermal collectors [12,13]. One shared drawback of the mentioned materials is their low thermal conductivity.

Different approaches have been investigated to improve this, while satisfying a sufficient mass transport. Thermal conductivity was increased by combining expanded graphite powders with silica gel powders and consolidating the mixture by compressive molding [14]. It was also proposed to use strontium chloride impregnated in expanded graphite [15]. Graphite foam has been also used in combination with SAPO-34 [16]. Metallic foams [17–19] and metallic fibers [20] have been previously used as substrates in adsorbers. Another approach was to reduce the heat transfer resistance by coating the zeolite powder directly on metallic heat exchanger surfaces [21–25]. The combination of adsorbents with the thermal conductivity of metals is one of the most promising alternatives to improve the overall performance of the adsorber.

In this study, for the first time, a systematic analysis of coated metallic heat exchangers with metallic salt hydrates was performed, including salt hydrates, which have not been described for the above-mentioned applications to date. The new materials were characterized by several physicochemical methods, such as thermogravimetric analysis (TGA), differential thermogravimetry (DTG), X-ray diffraction (XRD), and temperature programmed desorption (TPD). Coated heat exchangers allow an optimal contact between the hydrate and the metal, which increases the global heat conductivity and satisfies an optimal heat transport. The increase of high average heat conductivity is required in order to create adsorbers with a sufficient power with a reduced volume. The analysis was divided into two steps: verification of adsorbent–substrate chemical compatibility and analysis of two novel coating methods. The objective was to find the process and materials that allow the production of a stable coated heat exchanger with significantly improved thermal conductivity.

The direct impregnation of salt hydrates on the metal from aqueous solutions leads to unstable composites due to a suboptimal adherence of the coating on the surface of the substrate. Slight bending or thermal expansion causes the separation and rupture of the coating from the metal. Two new coating methods were studied to overcome these drawbacks. In one, the hydrates were synthesized directly on the surface of the metal by the reaction of an acid or mixture of acids with the substrate. Alternatively, a polymer was used to improve the stability of the coating. Polyvinyl alcohol (PVOH) was chosen as the binding material because it has been previously successfully applied in similar situations [26]. A systematic study of novel composites of this binder in combination with hydrates was performed. The results from the combination of PVOH and the salts were tested mechanically and compared to the corresponding coatings with pure salts.

## 2. Materials and Methods

The selection of materials was made according to their suitability for refrigeration systems or heat pumps. The selection of metallic salts was made according to their capacity of desorbing a meaningful amount of water at temperatures around 100 °C. Aluminum sulfate ( $\text{Al}_2(\text{SO}_4)_3$ ) has interesting properties for implementation in adsorption refrigeration, heating, and storage [27–29], but its application in these fields has been scarcely investigated [30]. Under vacuum conditions, the salt is reported to lose two molecules of water at around 80 °C, with a reaction enthalpy of 74.64 kJ/mol of desorbed water. The TGA results show that the dehydration occurs in three steps, as shown in Figure 1. It reveals that the material is almost dehydrated at around 450 °C. However, at 125.3 °C, a mass loss of 34.3% can be expected, which corresponds to a release of 13 water molecules. The remaining water evaporated at 359 °C, which corresponds to one molecule water. Aluminum sulfate octadecahydrate CAS-Nr. 7784-31-8 100–110% was used (Sigma Aldrich, Saint Louis, MO, USA).

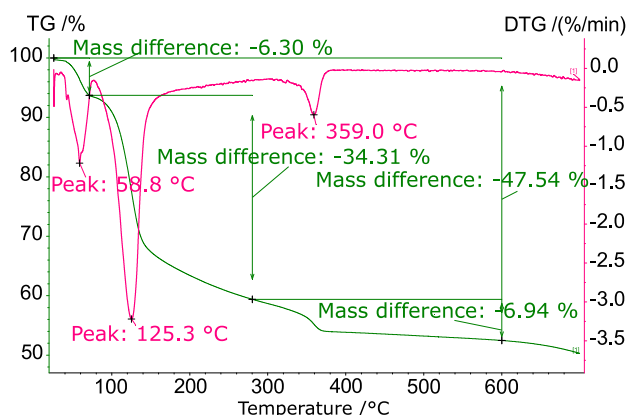


**Figure 1.** Thermogravimetric analysis/differential thermogravimetry (TGA/DTG) experimental result of  $\text{Al}_2(\text{SO}_4)_3 \cdot x\text{H}_2\text{O}$  heating showing its capacity for dehydration at low temperatures: 34.3% of its mass was lost below 125.3 °C.

Anhydrous magnesium sulfate ( $\text{MgSO}_4$ ) exists in three modifications, the  $\alpha$ ,  $\beta$ , and  $\gamma$  magnesium sulfate; however, in its dehydrated form, the  $\beta$ -form is the preferred modification [31]. Magnesium sulfate can be found in different hydration stages in naturally occurring minerals. The best known is the heptahydrate, called epsomite. A theoretical heat storage density of  $2.80 \text{ kJ} \cdot \text{cm}^{-3}$  for heat storage applications can be reached for the reaction from the anhydrous salt to the heptahydrate [32]. However, the full dehydration to the anhydrous material occurs above 200 °C; therefore, this reaction cannot be used for low temperature applications [30]. For temperatures below 150 °C, the reversible reaction from the monohydrate to heptahydrate with a calculated storage density of about  $2.28 \text{ kJ} \cdot \text{cm}^{-3}$  is suitable for heat storage applications. Magnesium sulfate is one of the most studied materials in the field of adsorption refrigeration/heating or energy storage [12,33,34]. Magnesium sulfate dry CAS-Nr. 7487-88-9 99% was used (Grüssing GmbH, Filsum, Niedersachsen, Germany).

Copper chloride ( $\text{CuCl}_2$ ) hydrates have also been studied in the field of energy storage [35]. The equilibrium curves provided by the van't Hoff equation combined with data from Donkers et al. [27] show that  $\text{CuCl}_2$  possesses the thermodynamic properties that make it suitable for applications in the range of medium temperature levels. It loses 20% of the weight below 100 °C under vacuum, which corresponds to the loss of two molecules of water, with a reaction enthalpy of  $106.54 \text{ kJ/kg}$ . Copper(II) chloride dehydrate CAS-Nr. 7447-39-4 99% was used (Grüssing GmbH, Filsum, Niedersachsen, Germany).

Copper sulfate ( $\text{CuSO}_4$ ) has been previously analyzed because of its adsorption properties and its suitability for energy storage applications [27,34,35], however, it has not yet been considered for implementation in refrigeration or heat pumps. Concerning the material stability over the cycles,  $\text{CuSO}_4$  showed a remarkable decrease in the kinetics after 13 cycles, and a final rehydration level of 35%. The salt undergoes two dehydration steps under 100 °C, which makes it suitable for low temperature heat sources. In each dehydration step, the hydrate loses two molecules of water at 52 and 86 °C, respectively, with a reaction enthalpy of around  $90 \text{ kJ/mol}$  each. Copper(II) sulfate pentahydrate CAS-Nr. 7758-99-8 > 99.0% was used (Sigma Aldrich, Saint Louis, MO, USA).

Ferrous chloride ( $\text{FeCl}_2$ ) has also not been previously considered for the construction of adsorbers, but it can be found in the literature with other candidates, in combination with water [27] and ammonia [2]. It is claimed to be able to release two molecules of water at a temperature of around 36 °C with an enthalpy of reaction of  $56.1 \text{ kJ/mol}$ , and other two molecules of water at a temperature of around 59 °C with an enthalpy of  $65.8 \text{ kJ/mol}$ . Iron(II) chloride tetrahydrate CAS-Nr. 13478-10-9 > 99.0% was used (Honeywell Fluka, Charlotte, NC, USA).

Iron sulfate ( $\text{FeSO}_4$ ) has interesting properties as an adsorbent [27,36,37], but no reference could be found in the literature regarding its application in refrigeration, heating, or energy storage. It releases three molecules of water at temperatures between 60 and 70 °C. Furthermore, three molecules can

be released, but higher temperatures are required (150 °C). Iron(II) sulfate heptahydrate CAS-Nr. 7782-63-0 99.5% was used (Grüssing GmbH, Filsum, Niedersachsen, Germany).

The adsorption properties of zinc chloride ( $\text{ZnCl}_2$ ) have been already investigated, in combination with both water and ammonia [2,38]. It is capable of adsorbing two molecules of ammonia at a temperature of 35 °C, with vapor pressures as low as 0.04 bar. Zinc(II) chloride CAS-Nr. 7646-85-7 dry > 98% was used (Honeywell Fluka, Charlotte, NC, USA).

Strontium chloride ( $\text{SrCl}_2$ ) has been investigated not only in absorption processes, but also in adsorption processes with water [27,39] and ammonia [2,4,40] as refrigerants. The release of ammonia (one to seven ammonia molecules) happens at a temperature of 95.3 °C, with an enthalpy of 40 kJ/mol of ammonia. Strontium chloride hexahydrate CAS-Nr. 10025-70-4 (purity 99–102%) was used (Sigma Aldrich, Saint Louis, MO, USA). This salt is labelled as dangerous (Category 1) because it causes serious eye damage/irritation.

Potassium carbonate ( $\text{K}_2\text{CO}_3$ ) is a highly promising and deeply investigated adsorbent in the field of thermal energy storage [41,42]. It loses 1.5 molecules of water at 104 °C with a vapor pressure of 20 mbar and an enthalpy around 65.8 kJ/mol of water.

Polyvinyl alcohol (PVOH) has been previously used as a binder of zeolites [26], but its application has not been extended to other adsorbents. Polyvinyl alcohol Mowiol 56–98 CAS-Nr. 9002-89-5 was used (Sigma Aldrich, Saint Louis, MO, USA).

The hydration levels of pure salts were confirmed by TGA measurements. Thermogravimetric analysis and differential thermogravimetry were performed using a simultaneous TGA/DTG vacuum-tight device (Netzsch TG 209 F1 Libra) to investigate the water sorption properties. The measurements were carried out in a flowing nitrogen atmosphere with a flow rate of 10 ml/min and a temperature ranging from 25 to 200 °C in an alumina crucible. The heating rate was 1 °C/min, where the sample mass varied between 8 and 10 mg with a resolution of 0.1 µg.

The phase stability after the synthesis of the composites was checked by XRD measurements. Powder X-ray diffraction was performed using a Bruker D8 Advance Powder Diffractometer in Bragg Brentano Geometry equipped with a one-dimensional silicon strip Lynikeye detector and  $\text{Cu-K}\alpha 1$  radiation ( $\lambda = 1.540619 \text{ \AA}$ ) under ambient conditions. The raw data were analyzed with the Diffrac-EVA Program from Bruker.

Ammonia desorption analysis was performed employing a homemade TPD device using 50–70 mg of material. The samples were activated inside the TPD reactor at 450 °C for 1 h, ammonia was added at a pressure of 0.8 Torr, and then desorption of ammonia was performed heating the sample from 20 to 550 °C at a rate of 1 °C/min.

### 3. Results

Different combinations of metal–metal salts were investigated. In the first section, the chemical compatibility of combinations is described. In the second part, the synthesis of hydrates by direct reaction with acids on the surface of the substrate is investigated. Finally, the third part comprises the results of the analysis of the composites resulting from the combination of PVOH and salt hydrates and compared with common solutions.

#### 3.1. Material Compatibility

Several salts appear to be incompatible in combination with some metals. Corrosion and unexpected reactions have been previously observed in adsorbents [43]. The hydrated salts were prepared in a water solution and impregnated on a plate of the metal subjected to testing. The solution was left to dry under ambient conditions and analyzed by X-ray diffraction.

The pictures in Figure 2 show the reactions of several salt hydrates with aluminum. Ferrous chloride ( $\text{FeCl}_2$ ) corroded the metallic plate, converting the substrate into powder after a few days. Zinc chloride ( $\text{ZnCl}_2$ ) reacted with the aluminum, releasing a gas that could be observed by the formation of bubbles in the sample. The color of the hydrate of iron sulfate ( $\text{FeSO}_4$ ) changed from green to brown

after recrystallization, probably as a result of its oxidation in contact with air. Potassium carbonate ( $K_2CO_3$ ) suffered a strong reaction with the substrate, releasing substantial amounts of gas in a short time. The reactions in the case of zinc can be explained by the galvanic series [44], which predict higher reactivity of aluminum than zinc. Other authors have encountered the problem of incompatibility between zinc salts and aluminum [45]. Reactions can also arise from impurities in the samples or from the interaction with the air.

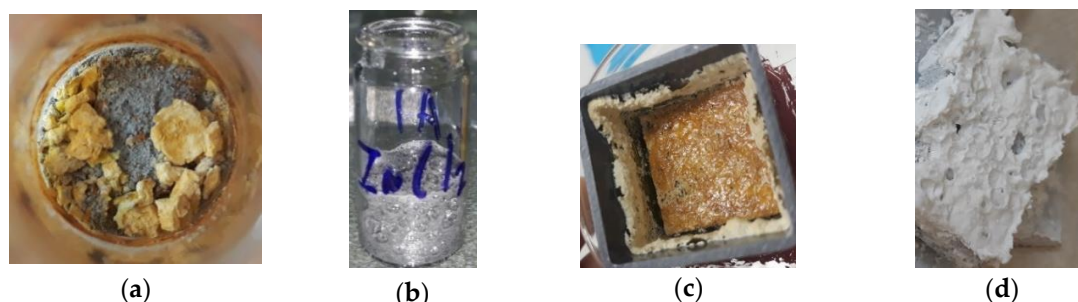


**Figure 2.** Effects of the incompatibility between (a)  $FeCl_2$ , (b)  $ZnCl_2$ , (c)  $FeSO_4$ , and (d)  $K_2CO_3$  with aluminum substrates.

The chemical compatibility of other salt–metal pairs could not be visually verified and they were subjected to XRD analysis. The results for the selected salts are discussed in detail next. Figure 3 illustrates the results of copper sulfate ( $CuSO_4$ ) in combination with aluminum. Copper sulfate hydrate was not among the species found in the sample:  $K_5H_3(SO_4)_4$  (potassium hydrogen sulfate),  $K_8(SO_4)(SO_3OH)_6$  (misenite),  $Al_2(SO_4)_3 \cdot 14H_2O$  (aluminum sulfate hydrate), and  $Cu_3(SO_4)0.5(OH) \cdot 5(H_2O)$  (montetrisaite). Several phases were formed as a result of the electrochemical difference between Cu and Al. The aimed phase  $CuSO_4 \cdot 5(H_2O)$  was not found among the products. Phases were found whose presence cannot be justified in this context, however, this does not affect the conclusion that copper sulfate and aluminum are incompatible.

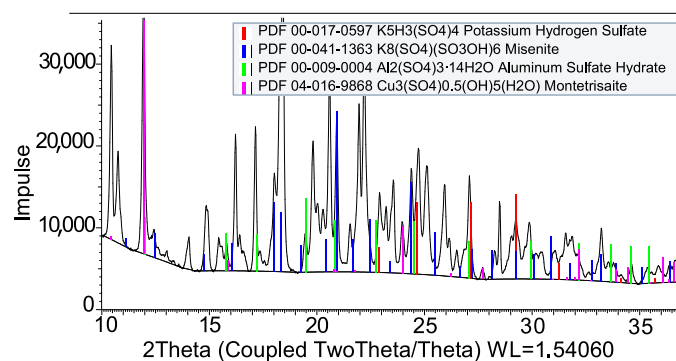


**Figure 3.** X-ray diffraction pattern of the composite  $CuSO_4/Al$ , verifying the absence of  $CuSO_4$  hydrate and the incompatibility of the salt with Al.

In contrast, magnesium sulfate ( $MgSO_4$ ) was found to be chemically stable in combination with aluminum. Figure 4 represents the diffraction pattern of the coating, which shows that only the desired hydrate was found.

Copper chloride ( $CuCl_2$ ) was tested in combination with copper. XRD analysis of the product revealed that there was a change of the chemical composition of the coating (see Figure 5). This X-ray diffraction pattern obtained at room temperature illustrates the presence of the following phases: clinoatacamite  $Cu_2Cl(OH)_3$  and acatamite  $Cu_2 + 2Cl(OH)_3$ . It can be concluded that the salt reacted during the coating process, which means that it cannot be added by wet impregnation.

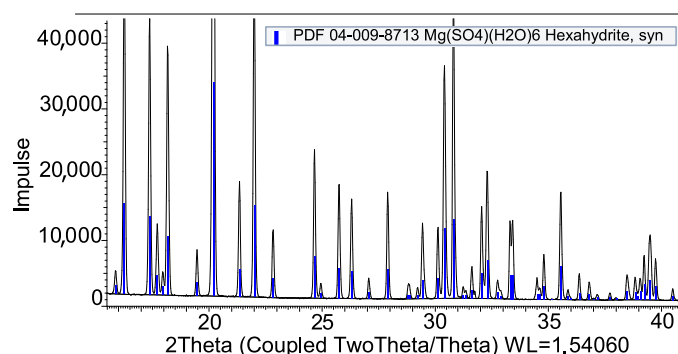


**Figure 4.** X-ray diffraction pattern of the composite  $\text{MgSO}_4/\text{Al}$ , verifying the presence of a single-phase hexahydrate  $\text{MgSO}_4 \cdot 6\text{H}_2\text{O}$  and its compatibility with Al.

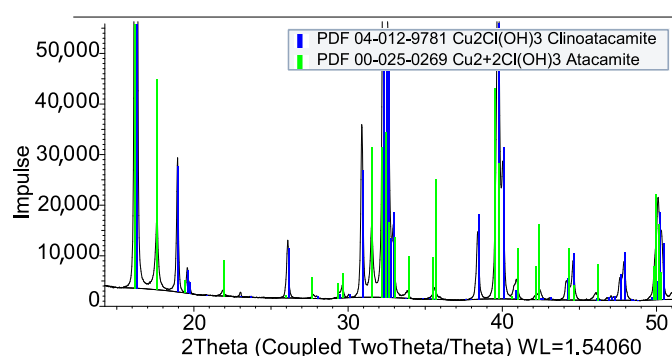


**Figure 5.** X-ray diffraction pattern of the composite  $\text{CuCl}_2/\text{Cu}$ , with the phases clinoatacamite and atacamite, proving the absence of the target hydrate  $\text{CuCl}_2 \cdot 2\text{H}_2\text{O}$ .

To avoid the reaction between salt and substrate, stainless steel was used in combination with the salts of iron. Figure 6 shows the resulting phases of the combination of ferrous chloride ( $\text{FeCl}_2$ ) and stainless steel (316L). At room temperature, the presence of the following phases could be found:  $\text{FeCl}_2 \cdot 4\text{H}_2\text{O}$ ,  $\text{Fe} + 3\text{O}(\text{OH})$  (akaganeite-Q), and  $\text{Fe}_3\text{O}_4$  (magnetite). No further phases were observed, indicating that the hydrate is compatible with steel.

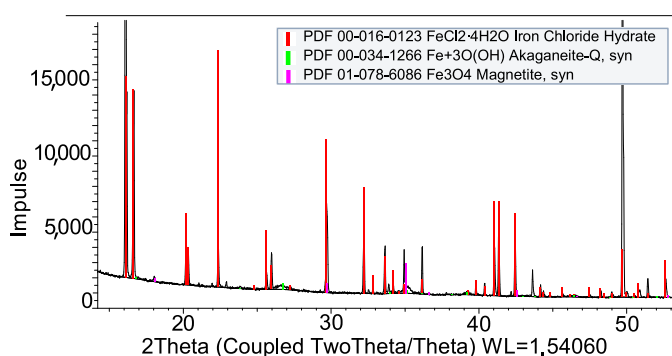


**Figure 6.** X-ray diffraction pattern of the composite  $\text{FeCl}_2/\text{SS-316L}$ , verifying the presence of the targeted  $\text{FeCl}_2 \cdot 4\text{H}_2\text{O}$ , which verifies the compatibility of the hydrate with 316L, and minor secondary species akaganeite and magnetite.

The combination of iron sulfate ( $\text{FeSO}_4$ ) with stainless steel created a coat without further chemical reactions, according to the X-ray diffraction represented in Figure 7. Only  $\text{Fe}(\text{SO}_4) \cdot 7(\text{H}_2\text{O})$  (melanterite) was detected, which proves the compatibility between the hydrate and the substrate 316L.

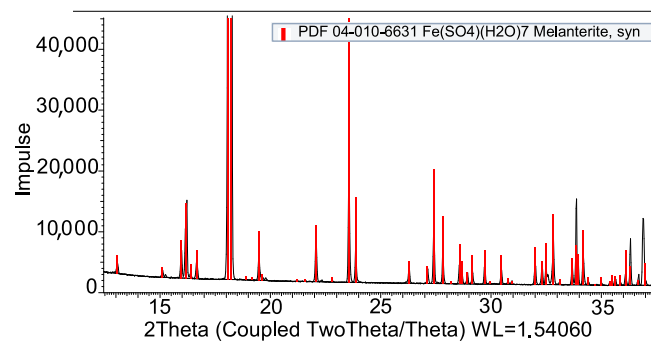


**Figure 7.** X-ray diffraction pattern of the composite  $\text{FeSO}_4/\text{SS-316L}$ , which verifies the presence of the targeted hydrate  $\text{Fe}(\text{SO}_4)\cdot 7\text{H}_2\text{O}$  and its compatibility with SS-316L.

In addition, potassium carbonate was tested in combination with stainless steel 316L. Two phases were detected in the XRD analysis (Figure 8):  $\text{K}_2\text{CO}_3\cdot 1.5\text{H}_2\text{O}$  was the main phase, with a minor secondary hydrate  $\text{K}_4\text{H}_2(\text{CO}_3)\cdot 1.5\text{H}_2\text{O}$  (potassium hydrogen carbonate hydrate). It can be concluded that stainless steel 316-L can be used as substrate for potassium carbonate.

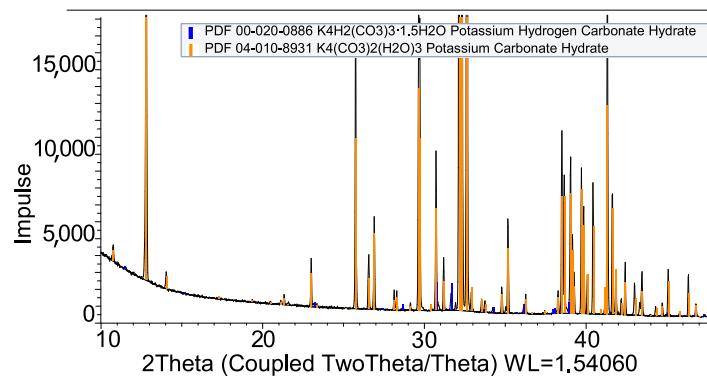


**Figure 8.** X-ray diffraction pattern of the composite  $\text{K}_2\text{CO}_3/\text{SS-316L}$ , which verifies the presence of the targeted hydrate  $\text{K}_2\text{CO}_3\cdot 1.5\text{H}_2\text{O}$  and its compatibility with 316L, with a minor secondary species potassium hydrogen carbonate hydrate.

### 3.2. Coating by Reaction

The adherence and general integrity of coatings obtained by impregnation appeared to be far from optimal. Minor mechanical impacts, such as slight bending of the metallic substrate, led in most cases to the loss of salt from the surface. Some examples of successful coating experiments with the new way of direct reaction with acid on the metal are given below.

The reaction of sulfuric acid with aluminum produced a stable and well-adhered layer of aluminum sulfate. Moreover, it was also possible to obtain very thin and uniform coats just by making a pretreatment of the surface with diluted sulfuric acid. Figure 9 illustrates the resulting sample with a coating of  $15 \text{ mg/cm}^2$ .



**Figure 9.**  $\text{Al}_2(\text{SO}_4)_3$  can be coated as uniform layers as thin as  $15 \text{ mg/cm}^2$  on a plate of Al.

The XRD analysis was performed after the synthesis of sulfuric acid 20% with aluminum and the following drying process (Figure 10). The main phases were  $\text{Al}_2(\text{SO}_4)_3 \cdot 17\text{H}_2\text{O}$  (alunogen) and  $\text{Al}_2(\text{SO}_4)_3 \cdot 12\text{H}_2\text{O}$  (meta-alunogen). As a minor phase,  $\text{Al}_2(\text{SO}_4)_3 \cdot 18\text{H}_2\text{O}$  (alumogenite) could be identified.

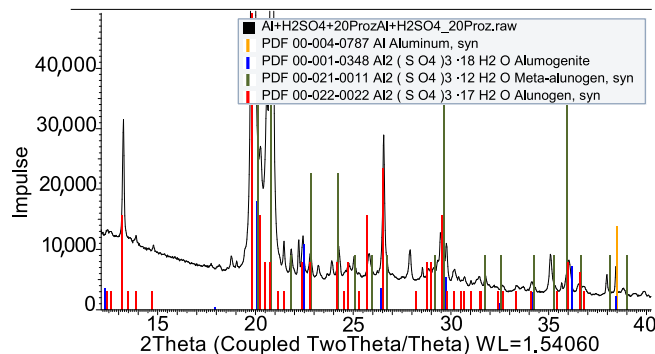


**Figure 10.** X-ray pattern of  $\text{H}_2\text{SO}_4 + \text{Al}$ , which verifies the presence of the targeted hydrate  $\text{Al}_2(\text{SO}_4)_3 \cdot \text{H}_2\text{O}$  plus lower hydrates and the suitability of the reaction for the coating process.

Aluminum chloride is not of special interest for application in heat pumps and refrigeration systems because of its high temperature of dehydration and the production of hydrochloric acid [46]. Its implementation as a composite by direct reaction on the surface of a metallic support can be successfully achieved with diluted hydrochloric acid, as confirmed by the X-ray diffraction analysis represented in Figure 11.

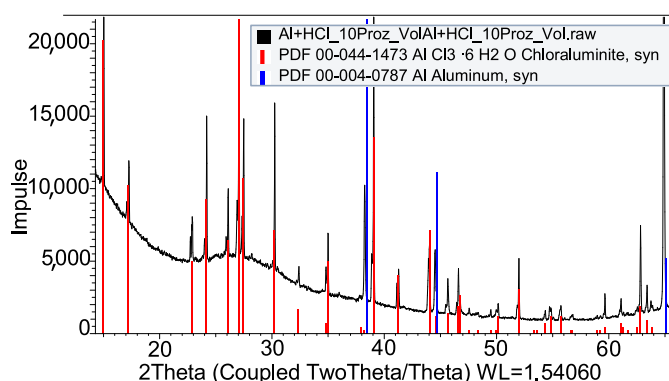


**Figure 11.** X-ray diffraction pattern of  $\text{Al} + \text{HCl}$ , which verifies the presence of the targeted hydrate  $\text{AlCl}_3 \cdot 6\text{H}_2\text{O}$  and the suitability of the reaction for the coating.

Aluminum is frequently used in the construction of heat exchangers because of its price and malleability. However, copper is usually preferred when high thermal conductivity and low heat capacity are required. Several salt hydrates of this metal possess interesting adsorption properties, as described in the introduction. Copper sulfate has very low temperatures of dehydration, which would be of great interest in the production of adsorbents driven by low temperature [27,47]. However, sulfuric acid does not easily react with copper because of passivation. It is necessary to make an initial reaction with nitric acid and the subsequent substitution of the nitric ions by sulfate ions. However, the replacement is not complete and secondary species can be found in the product. The XRD results can be seen in Figure 12, showing the phases after this special treatment. The poor reactivity and the difficulties found during the coating by reaction are caused by the formation of a passivation layer, which prevented the formation of sufficient amounts of the targeted hydrate.

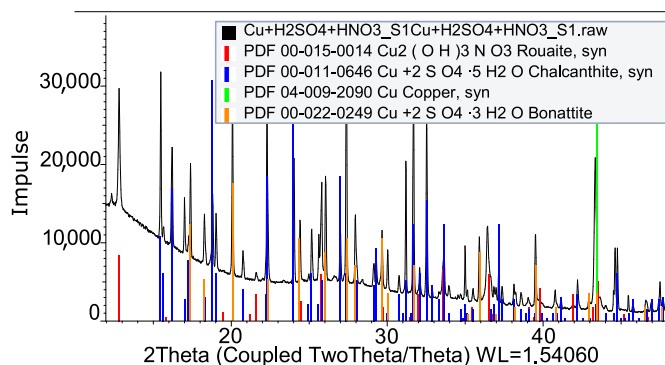


**Figure 12.** X-ray diffraction pattern of Cu + HNO<sub>3</sub> + H<sub>2</sub>SO<sub>4</sub>, which proves the presence of secondary species rouaite among the targeted hydrates chalcantite and bonattite.

Alternatively, coatings of copper chloride can be easily achieved by the reaction of diluted hydrochloric acid on the surface of copper. The effectiveness of the reaction was verified by XRD analysis. The direct synthesis of 10% hydrochloric acid on Cu-metal leads to the formation of the oxidized hydrate phase CuCl<sub>2</sub>·2H<sub>2</sub>O (eriochalcite), as shown in Figure 13. The phases detected in the products of the reaction were CuCl (nantokite) and hydrate phase CuCl<sub>2</sub>·2H<sub>2</sub>O (eriochalcite). It can be concluded that the reaction can be used to coat metals with the targeted hydrate.

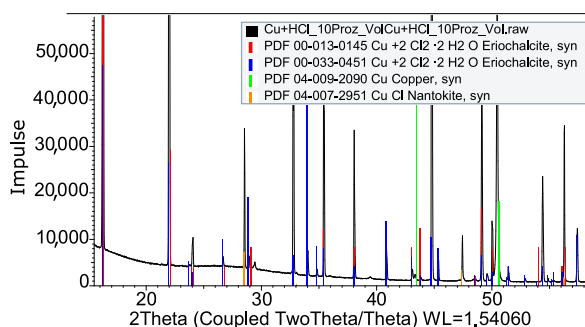


**Figure 13.** X-ray diffraction pattern of Cu + HCl, which verifies the presence of the targeted hydrate CuCl<sub>2</sub>·2H<sub>2</sub>O and the suitability of the reaction for the coating process, with minor secondary species nantokite.

### 3.3. Composites with Binding Material

Some of the composites were chemically stable but had poor mechanical stability due to weak adherence of the hydrate on the surface of the metal. To overcome this drawback, a polymer was added to increase both the adherence of the coat and the flexibility of the coating. Polyvinyl alcohol (PVOH) was the selected polymer for this new procedure.

Magnesium sulfate (MgSO<sub>4</sub>) is one of the most interesting salts owing to its thermodynamic properties. Because of the great potential of the hydrate, it was one of the salts selected to be combined with PVOH. A preparation from a single impregnation with a water solution of magnesium sulfate and polymer led to a heterogeneous coat with a sandwich-like structure consisting of a salt-rich layer trapped between two polymer-rich layers (see Figure 14). Alternative impregnations of magnesium sulfate and polymer yielded a more homogenous coating (see Figure 15). With a content of polymer of 20%, the integrity of the salt was strongly improved, but the adherence was still not sufficient to resist the installation of the coated fin in a heat exchanger; the process made the layer fall from the surface.

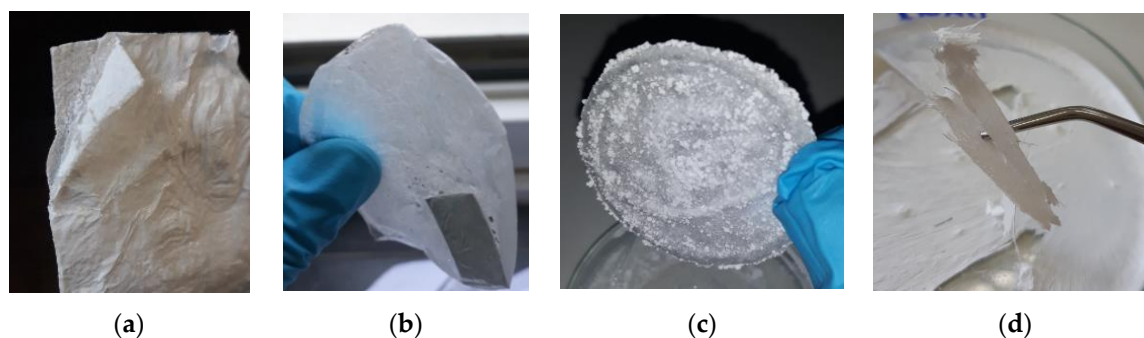


**Figure 14.** Macroscopic properties and stability of (a)  $\text{MgSO}_4$ , (b)  $\text{Al}_2(\text{SO}_4)_3$ , (c)  $\text{K}_2\text{CO}_3$ , and (d)  $\text{SrCl}_2$  with polyvinyl alcohol (PVOH).



**Figure 15.** Composite  $\text{MgSO}_4$ -hydrate/PVOH with improved stability.

It was examined whether the addition of PVOH had an influence on the chemical composition of the final coating. The X-ray diffraction pattern obtained at room temperature showed the presence of the following phases:  $\text{MgSO}_4 \cdot 4\text{H}_2\text{O}$  (starkeyite), hexahydrate  $\text{MgSO}_4 \cdot 6\text{H}_2\text{O}$ , and  $\text{Mg}(\text{OH})_2$  brucite (Figure 16), and thus a phase mixture of different hydrates.

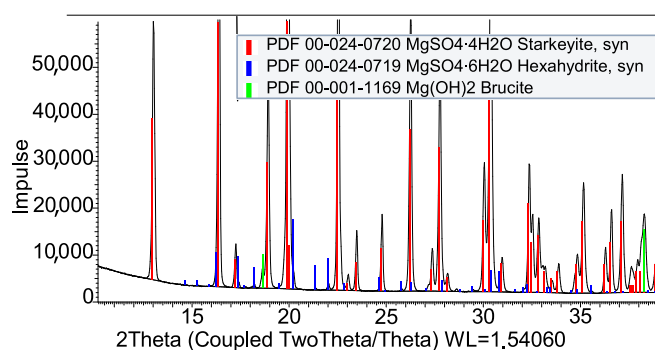


**Figure 16.** X-ray diffraction pattern of the composite  $\text{MgSO}_4$ /PVOH, which proves the presence of the targeted hydrate  $\text{MgSO}_4 \cdot \text{H}_2\text{O}$  and its compatibility with PVOH.

The sorption behavior of water on  $\text{MgSO}_4$  was investigated using TGA and DTG. The shape of the TGA curve shows that the mass loss occurs in three steps, each accompanied by a DTG signal (Figure 17). The first step occurs at a low temperature ( $33.3^\circ\text{C}$ ), involving a mass loss of 15%. All of the DTG peaks are negative, which shows that the steps are endothermic. The second dehydration step occurs between 25 and  $55^\circ\text{C}$ , and the third one between 60 and  $90^\circ\text{C}$ . The first peak corresponds to the loss of one water molecule, which occurs normally at about  $25^\circ\text{C}$  [27]. This corresponds to the XRD pattern, which shows  $\text{MgSO}_4 \cdot 6\text{H}_2\text{O}$  as the main phase and  $\text{MgSO}_4 \cdot 2\text{H}_2\text{O}$  as the minor phase. From the asymmetric shape of the TG curve, it is concluded that the second dehydration step consists of at least two hydration steps: at first, a signal can be observed indicating an initial loss of weight, followed by a more gradual decrease. The sharp drop in mass corresponds to a loss of approximately four water molecules; this suggests that the dehydration of  $\text{MgSO}_4 \cdot 6\text{H}_2\text{O}$  occurs in

two steps. It is suggested that the dehydration of  $\text{MgSO}_4 \cdot 6\text{H}_2\text{O}$  proceeds through the intermediate phase  $\text{MgSO}_4 \cdot 2\text{H}_2\text{O}$ . However, the XRD pattern showed that the dihydrate is already formed at room temperature, indicating a more complex mechanism of dehydration. Regardless, the comparison of the thermogravimetric analysis with the literature [48] proved that the dehydration of the composite is similar to that expected from the pure salt. This means that the thermodynamic properties of the hydrate are not influenced by the combination of the salt with the polymer.

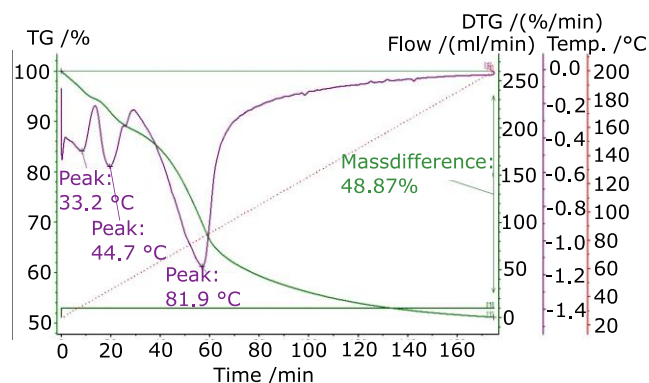


**Figure 17.** TGA/DTG of  $\text{MgSO}_4/\text{PVOH}$ ; lilac: DTG, green: TGA, which proves the lack of influence of the polymer in the desorption properties of the hydrate.

The combination of aluminum sulfate with polyvinyl alcohol (10%) was considered to provide additional stability of the coating (Figure 14). The observed films were flexible and had an improved adherence to the metal compared with the pure salts. The film presented good resistance to bending, in addition to good adherence to the metal. The presence of aluminum sulfate hydrates after synthesis with the polymer was verified by XRD. Figure 18 illustrates the XRD pattern of the composite.  $\text{Al}_2(\text{SO}_4)_3 \cdot 17\text{H}_2\text{O}$  (alunogen) and  $\text{Al}_2(\text{SO}_4)_3 \cdot 14\text{H}_2\text{O}$  (meta-alunogen) were observed in the sample, proving the presence of the hydrates of interest for the construction of an adsorber.

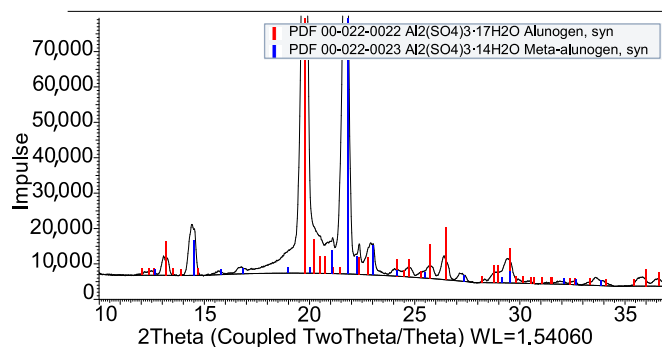


**Figure 18.** X-ray diffraction pattern of composite  $\text{Al}_2(\text{SO}_4)_3/\text{PVOH}$ , which proves the presence of the targeted hydrate  $\text{Al}_2(\text{SO}_4)_3$  with lower hydrates and their compatibility with PVOH.

Potassium carbonate ( $\text{K}_2\text{CO}_3$ ) also created a robust composite in combination with PVOH. The product also presents some heterogeneity, but with proportions as low as 15% PVOH, it presents a remarkable integrity (see Figure 14).

Strontium chloride ( $\text{SrCl}_2$ ) was also mixed with just 10% PVOH, creating weak films (see Figure 19). The product was analyzed by XRD to detect any possible reaction between the salt and the polymer. Only the species strontium chloride hydrate was detected, proving that both compounds are compatible.

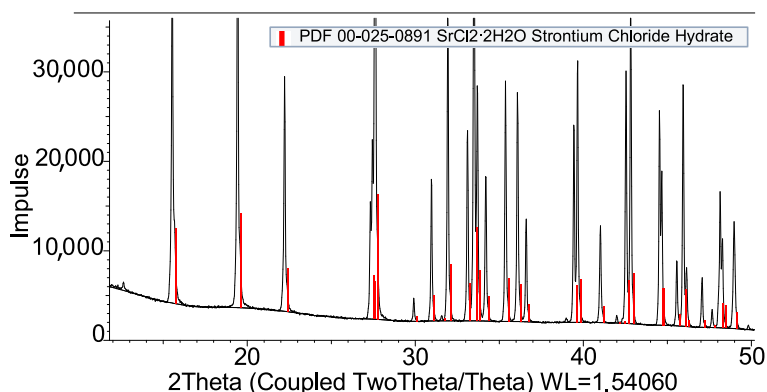


**Figure 19.** X-ray diffraction pattern of composite SrCl<sub>2</sub>/PVOH, which proves the presence of the targeted hydrate SrCl<sub>2</sub>·2H<sub>2</sub>O and its compatibility with PVOH.

### 3.4. TPD

The desorption of ammonia was investigated for one sample. Ammonia was adsorbed in CuCl and then desorbed under controlled temperature conditions.

Desorption of ammonia was followed by infrared spectroscopy (IR). Figure 20 shows a band at 3239 cm<sup>-1</sup>, which is characteristic of the existence of a bonding of NH<sub>3</sub>-CuCl (Figure 20). Additionally, a band at 1230 cm<sup>-1</sup> was observed, which is also characteristic of a vibration of this bond. The absence of bands at 2830 and 3050 cm<sup>-1</sup> means that no NH<sub>4</sub>Cl was formed. The desorption of NH<sub>3</sub> at 152 °C failed, although it is far from a theoretically expected desorption.

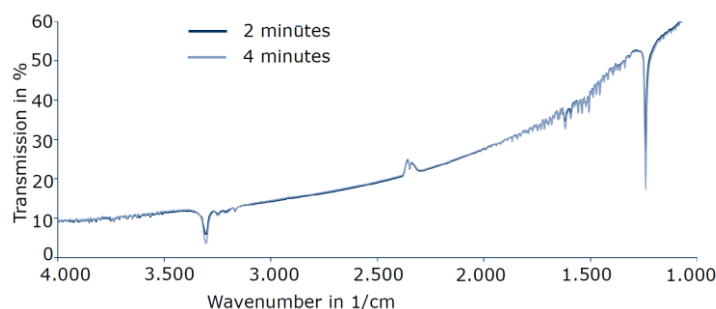


**Figure 20.** Temperature programmed desorption (TPD) experiments with CuCl and ammonia.

## 4. Discussion

In this paper, inorganic salts were deposited on metals to form stable composites with the aim of creating working pairs for potential applications in adsorption cooling machines and heat pumps. Initially, it was shown that solutions of different chlorides, sulfates of aluminum, copper, and K<sub>2</sub>CO<sub>3</sub> on aluminum substrates lead to corrosive effects and the creation of foreign phases.

Therefore, the coating of pure salt hydrates was performed by different methods on the corresponding metals. The exception was MgSO<sub>4</sub> on aluminum, which, by impregnation of an aqueous solution of MgSO<sub>4</sub> on aluminum, showed the formation of the six-fold Mg-hydrated phase. A solution of FeSO<sub>4</sub> on stainless steel showed the formation of the highest hydrated forms, suitable for direct use in adsorption–desorption processes.

The direct reaction of acids with the surface of metals led to an improved fixation of the salt hydrate on the metal. The best results were found for the reactions of sulfuric and hydrochloric acid on aluminum, leading to high hydrated phases. The reaction of a mixture of nitric and hydrochloric acid with copper led to the formation of a mixture of the pentahydrate and trihydrate sulfate phases and minor foreign phases. Before using these working pairs in the application of adsorption–desorption processes, further hydration must be performed to remove the tri-hydrated phase.

The application of PVOH as a polymeric binder was successfully applied to form a stable sheet of salt hydrates incorporated into the polymer phase on the metal. The main advantage of this method is to form metal–salt pairs, where corrosive effects or the formation of foreign phases make these metal–salt working pairs normally unsuitable for their application in adsorption–desorption processes. The method can be successfully applied to the combination of  $\text{Al}_2(\text{SO}_4)_3$ ,  $\text{MgSO}_4$ , and  $\text{SrCl}_2$  with PVOH. The size extension of the composite of  $\text{Al}_2(\text{SO}_4)_3/\text{PVOH}/\text{Al}$  to technological scale showed a strong binding of the composite on the metal showing a high mechanical stability towards bending and vibrations. Table 1 summarizes the conclusions of the analysis presented in this work.

**Table 1.** Material analysis. PVOH, polyvinyl alcohol.

Impregnation	
Salt + Metal	Compatibility
$\text{FeCl}_2 + \text{Al}$	Not compatible
$\text{ZnCl}_2 + \text{Al}$	Not compatible
$\text{FeSO}_4 + \text{Al}$	Not compatible
$\text{K}_2\text{CO}_3 + \text{Al}$	Not compatible
$\text{CuSO}_4 + \text{Al}$	Not compatible
$\text{MgSO}_4 + \text{Al}$	Compatible
$\text{CuCl}_2 + \text{Cu}$	Not compatible
$\text{FeCl}_2 + \text{SS-316L}$	Compatible
$\text{Fe}(\text{SO}_4) + \text{SS-316L}$	Compatible
$\text{K}_2\text{CO}_3 + \text{SS-316L}$	Compatible
Direct reactions	
Reactants	Products
$\text{H}_2\text{SO}_4 + \text{Al}$	$\text{Al}_2(\text{SO}_4)_3 \cdot 16\text{H}_2\text{O}$
$\text{HCl} + \text{Al}$	$\text{AlCl}_3 \cdot 6\text{H}_2\text{O}$
$\text{HNO}_3 + \text{H}_2\text{SO}_3 + \text{Cu}$	Not valid
$\text{HCl} + \text{Cu}$	$\text{CuCl}_2 \cdot 2\text{H}_2\text{O}$
Composites	
Salt + Composite	Compatibility
$\text{MgSO}_4 + \text{PVOH}$	Compatible
$\text{Al}_2(\text{SO}_4)_3 + \text{PVOH}$	Compatible
$\text{SrCl}_2 + \text{PVOH}$	Compatible

The selection of the most suitable salt for each application should then be made according to the thermodynamic properties of the corresponding salts and the boundary conditions of the specific process. The results presented in this work represent an extensive analysis of the material compatibility, from the chemical point of view, of some of the most interesting salt hydrates. In addition, two novel coating methods were explored, which can improve the stability of coated adsorbers. The selection of the most suitable method in each case will be then based on the chemical compatibility of the corresponding hydrate and/or the specific metallic substrate, and the purpose of the heat exchanger, that is, high power or high capacity.

**Author Contributions:** Conceptualization, C.B and S.O.; methodology, O.B.; software, V.P. and M.G.; validation, V.P., M.G., F.A., and M.V.; formal analysis, O.B.; investigation, O.B.; resources, C.B.; data curation, C.B.; writing—original draft preparation, S.O.; writing—review and editing, O.B. and C.B.; visualization, O.B.; supervision, C.B.; project administration, S.O.; funding acquisition, C.B. All authors have read and agreed to the published version of the manuscript.

**Funding:** This research was funded by Bundesministerium für Wirtschaft und Technologie, grant number 03ET1451A.

**Acknowledgments:** We thank the Fraunhofer Institute for Manufacturing Technology and Advanced Materials IFAM Dresden for their collaboration.

**Conflicts of Interest:** The authors declare no conflict of interest. The funders had no role in the design of the study; in the collection, analyses, or interpretation of data; in the writing of the manuscript; or in the decision to publish the results.

## References

1. Wang, R.; Oliveira, R.G. Adsorption refrigeration—An efficient way to make good use of waste heat and solar energy. *Prog. Energy Combust. Sci.* **2006**, *32*, 424–458. [[CrossRef](#)]
2. Wang, R.Z.; Wang, L.W.; Wu, J.Y. *Adsorption Refrigeration Theory and Applications*; Wiley: Hoboken, NJ, USA, 2014.
3. Dias, J.M.; Costa, V.A.F. Adsorption heat pumps for heating applications: A review of current state, literature gaps and development challenges. *Renew. Sustain. Energy Rev.* **2018**, *98*, 317–327. [[CrossRef](#)]
4. Jiang, L.; Wang, L.; Luo, W.; Wang, R. Experimental study on working pairs for two-stage chemisorption freezing cycle. *Renew. Energy* **2015**, *74*, 287–297. [[CrossRef](#)]
5. Cabeza, L.F.; Sole, A.; Cabeza, L.F. Review on sorption materials and technologies for heat pumps and thermal energy storage. *Renew. Energy* **2017**, *110*, 3–39. [[CrossRef](#)]
6. Scapino, L.; Zondag, H.A.; Van Bael, J.; Diriken, J.; Rindt, C.C. Sorption heat storage for long-term low-temperature applications: A review on the advancements at material and prototype scale. *Appl. Energy* **2017**, *190*, 920–948. [[CrossRef](#)]
7. Henninger, S.K.; Jeremias, F.; Kummer, H.; Schossig, P.; Henning, H.-M. Novel Sorption Materials for Solar Heating and Cooling. *Energy Procedia* **2012**, *30*, 279–288. [[CrossRef](#)]
8. Aristov, Y. Challenging offers of material science for adsorption heat transformation: A review. *Appl. Therm. Eng.* **2013**, *50*, 1610–1618. [[CrossRef](#)]
9. Freni, A.; Bonaccorsi, L.; Calabrese, L.; Capri, A.; Frazzica, A.; Sapienza, A. SAPO-34 coated adsorbent heat exchanger for adsorption chillers. *Appl. Therm. Eng.* **2015**, *82*, 1–7. [[CrossRef](#)]
10. Rammelberg, H.U.; Osterland, T.; Priehs, B.; Opel, O.; Ruck, W.K. Thermochemical heat storage materials—Performance of mixed salt hydrates. *Sol. Energy* **2016**, *136*, 571–589. [[CrossRef](#)]
11. Lee, J.S.; Yoon, J.W.; Mileo, P.G.M.; Cho, K.H.; Park, J.; Kim, K.; Kim, H.; De Lange, M.F.; Kapteijn, F.; Maurin, G.; et al. Porous Metal–Organic Framework CUK-1 for Adsorption Heat Allocation toward Green Applications of Natural Refrigerant Water. *ACS Appl. Mater. Interfaces* **2019**, *11*, 25778–25789. [[CrossRef](#)]
12. N'Tsoukpoe, K.E.; Schmidt, T.; Rammelberg, H.U.; Watts, B.A.; Ruck, W.K. A systematic multi-step screening of numerous salt hydrates for low temperature thermochemical energy storage. *Appl. Energy* **2014**, *124*, 1–16. [[CrossRef](#)]
13. Yu, N.; Wang, R.; Wang, L. Sorption thermal storage for solar energy. *Prog. Energy Combust. Sci.* **2013**, *39*, 489–514. [[CrossRef](#)]
14. Guilleminot, J.J.; Chalfen, J.B.; Poyelle, F. Transfers de masse et de chaleur dans les composites adsorbent consolidés. Influence sur les performances d'une pompe à chaleur à adsorption solide. In Proceedings of the 19th International Conference of Refrigeration, The Hague, The Netherlands, 20–25 August 1995.
15. Yuan, Y.; Bao, H.S.; Ma, Z.; Lu, Y.; Roskilly, A.P. Investigation of equilibrium and dynamic performance of SrCl<sub>2</sub>-expanded graphite composite in chemisorption refrigeration system. *Appl. Therm. Eng.* **2019**, *147*, 52–60. [[CrossRef](#)]
16. Bonaccorsi, L.; Bruzzaniti, P.; Calabrese, L.; Freni, A.; Proverbio, E.; Restuccia, G. Synthesis of SAPO-34 on graphite foams for adsorbent heat exchangers. *Appl. Therm. Eng.* **2013**, *61*, 848–852. [[CrossRef](#)]
17. Bonaccorsi, L.; Proverbio, E.; Freni, A.; Restuccia, G. In situ Growth of Zeolites on Metal Foamed Supports for Adsorption Heat Pumps. *J. Chem. Eng. Jpn.* **2007**, *40*, 1307–1312. [[CrossRef](#)]
18. Freni, A.; Bonaccorsi, L.; Proverbio, E.; Maggio, G.; Restuccia, G. Zeolite synthesised on copper foam for adsorption chillers: A mathematical model. *Microporous Mesoporous Mater.* **2009**, *120*, 402–409. [[CrossRef](#)]
19. Zhao, C.; Wu, Z. Heat transfer enhancement of high temperature thermal energy storage using metal foams and expanded graphite. *Sol. Energy Mater. Sol. Cells* **2011**, *95*, 636–643. [[CrossRef](#)]
20. Wittstadt, U.; Fuldner, G.; Andersen, O.; Herrmann, R.; Schmidt, F.P. A New Adsorbent Composite Material Based on Metal Fiber Technology and Its Application in Adsorption Heat Exchangers. *Energies* **2015**, *8*, 8431–8446. [[CrossRef](#)]

21. Fortes, A.D.; Wood, I.G.; Vočadlo, L.; Brand, H.E.A.; Knight, K.S. Crystal structures and thermal expansion of  $\alpha$ -MgSO<sub>4</sub> and  $\beta$ -MgSO<sub>4</sub> from 4.2 to 300 K by neutron powder diffraction. *J. Appl. Crystallogr.* **2007**, *40*, 761–770. [[CrossRef](#)]
22. Freni, A.; Frazzica, A.; Dawoud, B.; Chmielewski, S.; Calabrese, L.; Bonaccorsi, L. Adsorbent coatings for heat pumping applications: Verification of hydrothermal and mechanical stabilities. *Appl. Therm. Eng.* **2013**, *50*, 1658–1663. [[CrossRef](#)]
23. Schnabel, L.; Tatlier, M.; Schmidt, F.; Erdem-Şenatalar, A.; Tatlier, M. Adsorption kinetics of zeolite coatings directly crystallized on metal supports for heat pump applications (adsorption kinetics of zeolite coatings). *Appl. Therm. Eng.* **2010**, *30*, 1409–1416. [[CrossRef](#)]
24. Calabrese, L.; Bonaccorsi, L.; Bruzzaniti, P.; Proverbio, E.; Freni, A. SAPO-34 based zeolite coatings for adsorption heat pumps. *Energy* **2019**, *187*, 115981. [[CrossRef](#)]
25. Saeed, A.; Al-Alili, A. A review on desiccant coated heat exchangers. *Sci. Technol. Built Environ.* **2016**, *23*, 136–150. [[CrossRef](#)]
26. Van Heyden, H.; Munz, G.; Schnabel, L.; Schmidt, F.; Mintova, S.; Bein, T. Kinetics of water adsorption in microporous aluminophosphate layers for regenerative heat exchangers. *Appl. Therm. Eng.* **2009**, *29*, 1514–1522. [[CrossRef](#)]
27. Donkers, P.; Sögütöglü, L.; Huinink, H.; Fischer, H.; Adan, O. A review of salt hydrates for seasonal heat storage in domestic applications. *Appl. Energy* **2017**, *199*, 45–68. [[CrossRef](#)]
28. Kahlenberg, V.; Braun, D.E.; Krüger, H.; Schmidmair, D.; Orlova, A. Temperature- and moisture-dependent studies on alunogen and the crystal structure of meta-alunogen determined from laboratory powder diffraction data. *Phys. Chem. Miner.* **2016**, *44*, 95–107. [[CrossRef](#)]
29. Çilgi, G.K.; Cetisli, H. Thermal decomposition kinetics of aluminum sulfate hydrate. *J. Therm. Anal. Calorim.* **2009**, *98*, 855–861. [[CrossRef](#)]
30. Van Essen, V.M.; Gores, J.C.; Bleijendaal, L.P.J.; Zondag, H.; Schuitema, R.; Bakker, M.; Van Helden, W.G.J. *Characterization of Salt Hydrates for Compact Seasonal Thermochemical Storage, Proceedings of the ASME 2009 3rd International Conference on Energy Sustainability, San Francisco, CA, USA, 19–23 July 2009*; ASME International: New York, NY, USA, 2009; Volume 2, pp. 825–830.
31. Fortes, A.D.; Wood, I.G.; Alfredsson, M.; Vočadlo, L.; Knight, K.S. The thermoelastic properties of MgSO<sub>4</sub>·7D<sub>2</sub>O (epsomite) from powder neutron diffraction and ab initio calculation. *Eur. J. Miner.* **2006**, *18*, 449–462. [[CrossRef](#)]
32. Grevel, K.-D.; Majzlan, J. Internally consistent thermodynamic data for magnesium sulfate hydrates. *Geochim. Cosmochim. Acta* **2009**, *73*, 6805–6815. [[CrossRef](#)]
33. Schuitema, R.; van Helden, W.G.J.; Zondag, H.A.; van Essen, V.M.; Bleijendaal, L.P.J.; Cot Gores, J.; Planje, W.; Epema, T.; Oversloot, H. Comparison of reactor concepts for thermochemical storage of solar heat. In *Proceedings of the 3rd International Renewable Energy Storage Conference (IRES 2008)*, Berlin, Germany, 24–25 November 2008.
34. Ferchaud, C.; Zondag, H.A.; de Boer, R.; Rindt CC, M. Characterization of the sorption process in thermochemical materials for seasonal solar heat storage application. In *Proceedings of the 12th international conference on energy storage (Innostock 2012)*, Lleida, Spain, 16–18 May 2012.
35. Donkers, P.; Pel, L.; Adan, O. Experimental studies for the cyclability of salt hydrates for thermochemical heat storage. *J. Energy Storage* **2016**, *5*, 25–32. [[CrossRef](#)]
36. Wang, T.; Debelak, K.A.; Roth, J.A. Dehydration of iron(II) sulfate heptahydrate. *Thermochim. Acta* **2007**, *462*, 89–93. [[CrossRef](#)]
37. Kanari, N.; Menad, N.-E.; Ostrosi, E.; Shallari, S.; Diot, F.; Allain, E.; Yvon, J. Thermal Behavior of Hydrated Iron Sulfate in Various Atmospheres. *Metals* **2018**, *8*, 1084. [[CrossRef](#)]
38. Fortier, H.; Westreich, P.; Selig, S.; Zelenietz, C.; Dahn, J. Ammonia, cyclohexane, nitrogen and water adsorption capacities of an activated carbon impregnated with increasing amounts of ZnCl<sub>2</sub>, and designed to chemisorb gaseous NH<sub>3</sub> from an air stream. *J. Colloid Interface Sci.* **2008**, *320*, 423–435. [[CrossRef](#)] [[PubMed](#)]
39. Harris, J.D.; Rusch, A.W. Identifying Hydrated Salts Using Simultaneous Thermogravimetric Analysis and Differential Scanning Calorimetry. *J. Chem. Educ.* **2012**, *90*, 235–238. [[CrossRef](#)]
40. Kuwata, K.; Masuda, S.; Kobayashi, N.; Fuse, T.; Okamura, T. Thermochemical Heat Storage Performance in the Gas/Liquid-Solid Reactions of SrCl<sub>2</sub> with NH<sub>3</sub>. *Nat. Resour.* **2016**, *7*, 655–665.

41. Gaeini, M.; Shaik, S.A.; Rindt, C.C.M. Characterization of potassium carbonate salt hydrate for thermochemical energy storage in buildings. *Energy Build.* **2019**, *196*, 178–193. [[CrossRef](#)]
42. Sögütöglü, L.; Donkers, P.; Fischer, H.; Huinink, H.; Adan, O. In-depth investigation of thermochemical performance in a heat battery: Cyclic analysis of K<sub>2</sub>CO<sub>3</sub>, MgCl<sub>2</sub> and Na<sub>2</sub>S. *Appl. Energy* **2018**, *215*, 159–173. [[CrossRef](#)]
43. D’Ans, P.; Courbon, E.; Frère, M.; Descy, G.; Segato, T.; Degrez, M. Severe corrosion of steel and copper by strontium bromide in thermochemical heat storage reactors. *Corros. Sci.* **2018**, *138*, 275–283. [[CrossRef](#)]
44. Farrell, A.J.; Norton, B.; Kennedy, D.M. Corrosive effects of salt hydrate phase change materials used with aluminium and copper. *J. Mater. Process. Technol.* **2006**, *175*, 198–205. [[CrossRef](#)]
45. Moreno, P.; Miró, L.; Sole, A.; Cabeza, L.F.; Solé, C.; Martorell, I.; Cabeza, L.F. Corrosion of metal and metal alloy containers in contact with phase change materials (PCM) for potential heating and cooling applications. *Appl. Energy* **2014**, *125*, 238–245. [[CrossRef](#)]
46. Zhang, N.; Yang, Y.; Wang, Z.; Shi, Z.; Gao, B.; Hu, X.; Tao, W.; Liu, F.; Yu, J. Study on the thermal decomposition of aluminium chloride hexahydrate. *Can. Met. Q.* **2017**, *57*, 235–244. [[CrossRef](#)]
47. Glasser, L. Thermodynamics of Inorganic Hydration and of Humidity Control, with an Extensive Database of Salt Hydrate Pairs. *J. Chem. Eng. Data* **2014**, *59*, 526–530. [[CrossRef](#)]
48. Van Essen, V.M.; Zondag, H.A.; Gores, J.C.; Bleijendaal, L.P.J.; Bakker, M.; Schuitema, R.; Van Helden, W.G.J.; He, Z.; Rindt, C.C.M. Characterization of MgSO<sub>4</sub> Hydrate for Thermochemical Seasonal Heat Storage. *J. Sol. Energy Eng.* **2009**, *131*. [[CrossRef](#)]



© 2020 by the authors. Licensee MDPI, Basel, Switzerland. This article is an open access article distributed under the terms and conditions of the Creative Commons Attribution (CC BY) license (<http://creativecommons.org/licenses/by/4.0/>).